CMS Physics Analysis Summary

Contact: cms-pag-conveners-susy@cern.ch 2013/05/13

Search for electroweak production of charginos, neutralinos, and sleptons using leptonic final states in pp collisions at $\sqrt{s} = 8\,\text{TeV}$

The CMS Collaboration

Abstract

(Note: This revision of the original 2012/11/27 document includes a correction in the same-sign analysis section.) Final states with exactly three leptons, four leptons, two same-sign leptons, two opposite-sign-same-flavor leptons plus two jets, and two opposite-sign leptons inconsistent with Z boson decay, are studied using a data sample consisting of an integrated luminosity of $9.2\,\text{fb}^{-1}$ of proton-proton collision data collected in 2012 with the CMS detector at $\sqrt{s} = 8$ TeV. The observed event rates are in agreement with expectations from the standard model. The results are used to set limits on the direct production of charginos, neutralinos, and sleptons. (The limits are unaffected by the same-sign analysis correction.)

1 Introduction

Many searches for supersymmetry (SUSY) [1–7] carried out at the CERN Large Hadron Collider (LHC) have focused on models with cross sections dominated by the production of strongly interacting new particles. The corresponding final states exhibit a high level of hadronic activity. In contrast, in this note, we describe searches motivated by the direct electroweak production of charginos, neutralinos, and sleptons. The corresponding final states do not necessarily contain much hadronic activity and thus may have eluded detection in other searches. This signature characterizes SUSY models that describe the pair production of charginos $\widetilde{\chi}^{\pm}$ and neutralinos $\widetilde{\chi}^{0}$, mixtures of the SUSY partners of the gauge and Higgs bosons, and of sleptons $\widetilde{\ell}$, the SUSY partners of leptons. Depending on the mass spectrum, the charginos and neutralinos can have significant decay branching fractions to leptons or on-shell vector bosons, yielding multilepton final states. Similarly, slepton pair production gives rise to final states with leptons. In all these cases, two stable, lightest-SUSY-particle (LSP) dark matter candidates are produced, which escape without detection, leading to significant missing transverse energy $E_{\mathrm{T}}^{\mathrm{miss}}$. Neutrinos present in the final state yield additional $E_{\mathrm{T}}^{\mathrm{miss}}$.

The studies presented in this note are based on a sample of proton-proton collision data collected at $\sqrt{s} = 8$ TeV with the CMS detector at the LHC in 2012, corresponding to an integrated luminosity of $9.2\,\mathrm{fb}^{-1}$. The study closely follows the procedures outlined in Ref. [8] and improves on those results. Additional details can be found in Ref. [9]. The new-physics scenarios we consider are shown in Figs. 1, 2 and 3. These figures are labeled using SUSY nomenclature, but the interpretation of our results can be extended to other new-physics models. In SUSY nomenclature, $\widetilde{\chi}_1^0$ is the lightest neutralino, presumed to be the LSP, $\widetilde{\chi}_2^0$ and $\widetilde{\chi}_3^0$ are heavier neutralinos, $\widetilde{\chi}_1^{\pm}$ is the lightest chargino, and $\tilde{\ell}$ is a slepton. In Fig. 1, the slepton mass $m_{\tilde{\ell}}$ is less than the masses $m_{\widetilde{\chi}_2^0}$ and $m_{\widetilde{\chi}_1^{\pm}}$, while in Fig. 2 it is greater. Also, for Fig. 2, the mass difference between the LSP and next-lightest chargino or neutralino is large enough to allow the production of on-shell W and Z bosons. Figure 3 shows diagrams for chargino- and slepton-pair production.

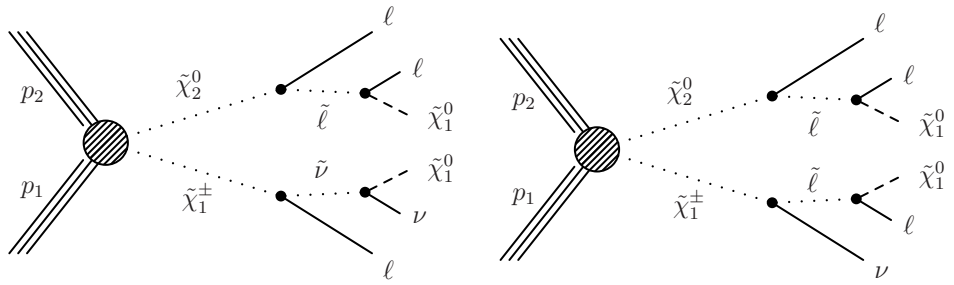

Figure 1: Chargino-neutralino production at LHC leading to a three-lepton final state with missing transverse energy $E_{\mathrm{T}}^{\mathrm{miss}}$. The dotted and dashed lines indicate unstable particles and the LSP, respectively.

The interpretation of our results is presented in the context of simplified model spectra (SMS). SUSY models with bino-like $\widetilde{\chi}_1^0$ and wino-like $\widetilde{\chi}_2^0$ and $\widetilde{\chi}_1^{\pm}$ yield the trilepton signature of Fig. 1, and motivate the simplifying assumption $m_{\widetilde{\chi}_2^0} = m_{\widetilde{\chi}_1^{\pm}}$ since these two gauginos belong to the same gauge-group multiplet. We thus present results as a function of the common $m_{\widetilde{\chi}_2^0} = m_{\widetilde{\chi}_1^{\pm}}$ mass and the LSP mass $m_{\widetilde{\chi}_1^0}$. The results for Fig. 1 also depend on the mass $m_{\tilde{\ell}}$ of the intermediate slepton (if left-handed, taken to be the same for its sneutrino $\tilde{\nu}$), parametrized in terms of

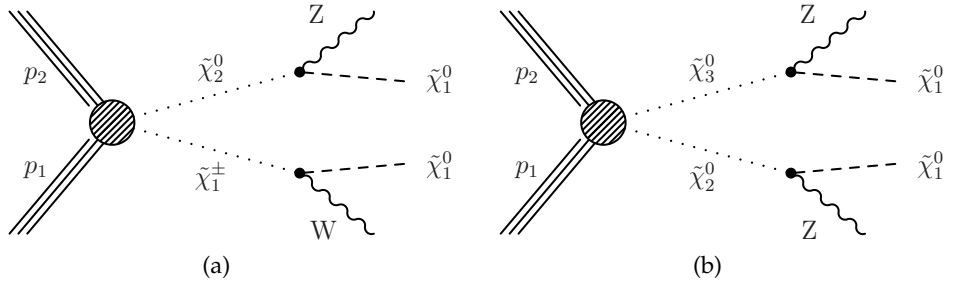

Figure 2: Chargino-neutralino and neutralino-neutralino production leading to on-shell W or Z bosons with $E_{\mathrm{T}}^{\mathrm{miss}}$.

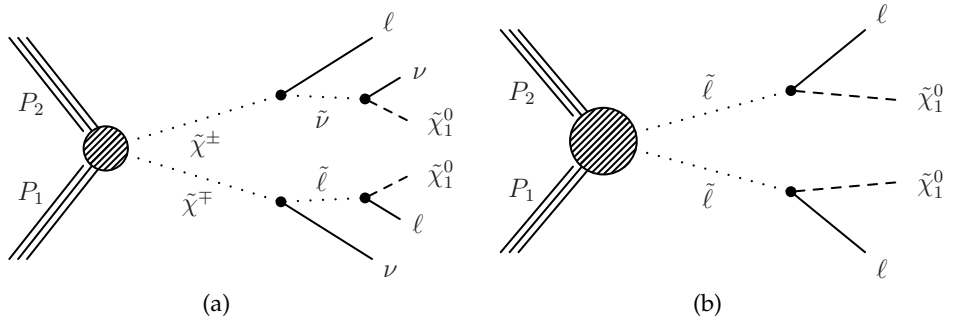

Figure 3: Chargino- and slepton-pair production leading to opposite-sign lepton pairs with $E_{\mathrm{T}}^{\mathrm{miss}}$. In the diagram of part (a), each chargino can decay via either mode, giving four possible diagrams sharing the same final state. In the diagram of part (b), the sleptons and thus the daughter leptons share the same flavor.

a variable $x_{\tilde{\ell}}$ as:

$$m_{\tilde{\ell}} = m_{\tilde{\chi}_1^0} + x_{\tilde{\ell}}\,(m_{\tilde{\chi}_1^\pm} - m_{\tilde{\chi}_1^0}), \tag{1}$$

where $0 < x_{\tilde{\ell}} < 1$. We present results for $x_{\tilde{\ell}}$ equal to 0.5 (i.e., the slepton mass equal to the mean of the LSP and chargino masses) and in some cases for $x_{\tilde{\ell}}$ =0.05 and 0.95.

The interpretation of the result may further depend on whether the sleptons are the SUSY partner $\widetilde{\ell}_L$ or $\widetilde{\ell}_R$ of left-handed or right-handed leptons. We consider two limiting cases. In one case, $\widetilde{\ell}_R$ does not participate while $\widetilde{\ell}_L$ and $\widetilde{\nu}$ do: then both diagrams of Fig. 1 exist, and the chargino and neutralino decay to all three lepton flavors with equal probability. Furthermore, two additional diagrams with $\tilde{\chi}_2^0 \to \ell\,\widetilde{\ell} \to \ell\,\ell\,\tilde{\chi}_1^0$ replaced by $\tilde{\chi}_2^0 \to \widetilde{\nu}\,\nu \to \nu\,\nu\,\tilde{\chi}_1^0$ reduce the fraction of three-lepton final states by 50%. In the second case, in which $\widetilde{\ell}_R$ participates while $\widetilde{\ell}_L$ and $\widetilde{\nu}$ do not, only the diagram of Fig. 1(b) exists, and there is no 50% loss of three-lepton final states. Because the $\widetilde{\ell}_R$ couples to the chargino via its higgsino component, chargino decays to $\widetilde{\ell}_R$ strongly favor the τ as the lepton. For the leptonic decay products, we thus consider three flavor scenarios:

- the "flavor-democratic" scenario: the chargino ($\tilde{\chi}_1^\pm$) and neutralino ($\tilde{\chi}_2^0$) both decay with equal probability into all three lepton flavors, as expected for $\widetilde{\ell}_L$;
- the "τ-enriched" scenario: the chargino decays exclusively to τ leptons as expected for $\widetilde{\ell}_R$, while the neutralino decays democratically;

- the "τ-dominated" scenario: the chargino and neutralino both decay only to a τ lepton.

We place limits on the pair-production cross section times branching fraction for the above scenarios. The 50% branching fraction to three leptons is taken into account when appropriate in $\widetilde{\ell}_L$ cases. For $x_{\widetilde{\ell}} = 0.5$, the kinematic conditions for the processes of Fig. 1 are identical for $\widetilde{\ell}_L$ and $\widetilde{\ell}_R$, and the respective limits are trivially related. For other values of $x_{\widetilde{\ell}}$, differences in experimental acceptance may alter the relationship, and are accounted for.

For results based on the diagrams of Fig. 2, there is little sensitivity to the ZZ channel of Fig. 2(b) because $\widetilde{\chi}_2^0$ and $\widetilde{\chi}_1^\pm$ are wino-like, which suppresses neutralino pair production relative to neutralino-chargino production. Therefore, for the ZZ signature, we consider a specific gauge-mediated supersymmetry breaking (GMSB) Z-enriched higgsino model [10–12] that enhances the $ZZ + E_{\mathrm{T}}^{\mathrm{miss}}$ final state. We assume that sleptons are too massive to participate, so that the branching fractions to vector bosons are 100%.

Figure 3(a) depicts chargino-pair production. For each event, each chargino can decay via either of the modes shown in the figure. Thus, there are four different decay pairs, but all yield a similar final state, with two opposite-sign leptons plus $E_{\mathrm{T}}^{\mathrm{miss}}$. For this model, we consider $x_{\widetilde{\ell}} = 0.50$ only. Figure 3(b) describes electron- and muon-slepton pair production, where each slepton decays to a lepton of the same flavor and to the LSP. We assume a universal mass for both slepton flavors.

In Section 2, we describe the data sample and event reconstruction procedures. Section 3 presents a search based on the three-lepton (electron, muon and tau) final state of Fig. 1. A search based on the four-lepton final state, again reconstructing all three lepton flavors and sensitive to the diagrams of Fig. 2(b), is presented in Section 4. Section 5 describes describes a search in a channel with exactly two same-sign dileptons, which augments sensitivity to the diagrams of Fig.1 in cases where one of the three leptons is not identified. In Section 6 we present a study based on on-shell W and Z bosons. This study is sensitive to the diagrams of Fig. 2. In Section 7, we present a search based on an opposite-sign, non-resonant dilepton pair, which is sensitive to the processes of Fig. 3. Section 8 presents an interpretation of these searches.

2 Detector, trigger, and object selection

The central feature of the CMS apparatus is a superconducting solenoid, of 6 m internal diameter, providing a magnetic field of 3.8 T. Within the field volume are a silicon pixel and strip tracker, a crystal electromagnetic calorimeter, and a brass-scintillator hadron calorimeter. Muons are measured in gas-ionization detectors embedded in the steel return yoke. Extensive forward calorimetry complements the coverage provided by the barrel and endcap detectors. A more detailed description can be found in Ref. [13].

CMS uses a right-handed coordinate system, with the origin at the nominal interaction point, the x axis pointing to the center of the LHC, the y axis pointing upwards (perpendicular to the plane of the LHC ring), and the z axis along the counterclockwise-beam direction. The polar angle θ is measured from the positive z axis, and the azimuthal angle ϕ (in radians) is measured in the x-y plane. The pseudorapidity η is defined by $\eta = -\ln[\tan(\theta/2)]$.

Events from pp interactions must satisfy the requirements of a two-level trigger system. The first level performs a fast selection for physics objects (jets, muons, electrons, and photons) above certain thresholds. The second level performs a full event reconstruction. The principal trigger used for this analysis requires at least one electron or muon with transverse momentum

$p_T > 17\,\text{GeV}$, another with $p_T > 8\,\text{GeV}$, and $|\eta| < 2.4$ for both electrons and muons.

Simulated event samples are used to study the characteristics of signal and standard model (SM) background. Most of the simulated event samples are produced with the MADGRAPH 5.1.1 [14, 15] event generator, with parton showering and hadronization performed with the PYTHIA 8.1 [16] program. Signal samples are generated with PYTHIA 6.424 [16]. The samples are generated using the CTEQ 6.6 [17] parton distribution functions. For the diboson backgrounds, MCFM [18] samples are used to help assess the theoretical uncertainties on the simulated samples. For the simulated SM samples, we use the most accurate calculations of the cross sections available, generally with next-to-leading order (NLO) accuracy [19–21]. The files specifying the SUSY signal model parameters are generated according to the SUSY Les Houches accord [22] standards with the ISAJET program [23], with cross sections calculated in PYTHIA to leading order and NLO corrections calculated using PROSPINO 2.1 [24]. For SM backgrounds, the detector response and reconstruction are modeled with the GEANT4 [25] program followed by the same event reconstruction as used for data. For signal models, the CMS fast simulation program [26] is used in place of GEANT.

Events are reconstructed offline using the particle-flow (PF) algorithm [27, 28], which provides a self-consistent global assignment of momenta and energies to the physics objects. Details of the reconstruction and identification procedures are given in Refs. [29, 30] for electrons and muons.

Jets are reconstructed with the anti-k_T clustering algorithm [31] with a distance parameter of 0.5. We apply p_T- and η-dependent corrections to account for residual effects of non-uniform detector response. The contribution to jet energy from multiple interactions in the event (pileup) is estimated on an event-by-event basis using the jet area method described in Ref. [32], and is subtracted from the overall jet p_T. We reject jets that are consistent with anomalous noise in the calorimeter detectors.

In order to suppress background from top-quark pair ($t\bar{t}$) production, events with jets originating from b quarks ("b jets") are rejected. This requirement suppresses $t\bar{t}$ background while avoiding signal loss from a more general jet veto. We use the combined-secondary-vertex algorithm [33] at the medium working point for b-jet identification. It has a b-jet tagging efficiency of 70% and a misidentification rate of 1%. Events with an identified b jet are rejected in the searches described below. With the exception of the search described in Section 5, which requires b jets to have $p_T > 40\,\text{GeV}$, the searches require b jets to have $p_T > 30\,\text{GeV}$.

Hadronic decays of the τ lepton are reconstructed using the "hadrons-plus-strips"algorithm [34, 35], which combines PF photon and electron candidates to form neutral pions. The neutral pions are combined with charged hadrons to form hadronic τ decay candidates.

Lepton (e, μ) candidates are required to share a common primary event vertex. Events with an opposite-sign ee or $\mu\mu$ pair with an invariant mass below 12 GeV are rejected in order to exclude quarkonia resonances, photon conversions, and low-mass continuum events. To reduce contamination due to leptons from heavy-flavor decay or misidentified hadrons in jets, leptons are required to be isolated. Electron and muon candidates are considered isolated if the ratio I_{rel} of the scalar sum of the transverse momenta of charged hadrons, photons, and neutral hadrons in a cone of $\Delta R = \sqrt{\Delta\eta^2 + \Delta\phi^2} = 0.3$ around the candidate, relative to the lepton p_T value, is less than 0.15. Jets must satisfy $|\eta| < 2.5$ and $p_T > 30\,\text{GeV}$ and lie $\Delta R > 0.4$ away from candidate leptons. Some of the searches presented below make use of the missing transverse energy E_T^{miss}, where E_T^{miss} is defined as the modulus of the vector sum of the transverse momenta of all PF objects. Similarly, some of the searches use the quantity H_T, defined as the

scalar sum of jet p_T values.

3 Search in the three-lepton final state

Three-lepton channels have sensitivity to models with signatures like those shown in Figs. 1 and 2. For the three-lepton search, we use reconstructed electrons, muons, and hadronically decaying τ leptons, all within $|\eta| < 2.4$. There must be at least one electron or muon with $p_T > 20\,\text{GeV}$. Other electrons or muons must have $p_T > 10\,\text{GeV}$. At most one hadronic τ is allowed and it must have $p_T > 20\,\text{GeV}$.

The principal backgrounds are from WZ production with three genuine isolated leptons that are "prompt" (created at the primary vertex), and from $t\bar{t}$ production with two genuine prompt leptons and a third non-prompt lepton misclassified as prompt.

Events are required to have $E_T^{miss} > 50\,\text{GeV}$. We consider events both with and without an opposite-sign-same-flavor (OSSF) lepton pair. Events with an OSSF pair are characterized by the invariant mass $M_{\ell\ell}$ of the pair and by the transverse mass M_T formed from the E_T^{miss} vector and the transverse momentum p_T^{ℓ} of the remaining lepton:

$$M_T \equiv \sqrt{2E_T^{miss} p_T^{\ell}[1 - \cos(\Delta\phi_{\ell,E_T^{miss}})]}. \quad (2)$$

For three-muon and three-electron events, the OSSF pair with $M_{\ell\ell}$ closer to the Z mass is used. For events without an OSSF pair, which might arise from events with a $Z \to \tau\tau$ decay, $M_{\ell\ell}$ is calculated by combining opposite-sign leptons and choosing the pair closest to the corresponding dilepton mass determined from $Z \to \tau\tau$ simulation (50 GeV for an eμ pair, or 60 GeV for a $\tau\mu$ or τe pair).

Events are classified into exclusive search regions ("bins") depending on their values of $M_{\ell\ell}$, E_T^{miss} and M_T. The $M_{\ell\ell}$ regions for OSSF dilepton pairs are [$M_{\ell\ell} < 75\,\text{GeV}$], [$75\,\text{GeV} < M_{\ell\ell} < 105\,\text{GeV}$], and [$105\,\text{GeV} < M_{\ell\ell}$]. Further event classification is in E_T^{miss} bins of [50,100], [100,150], [150,200], and [> 200] GeV. Finally, the M_T regions are [<120], [120-160], and [>160] GeV.

3.1 Background estimation

Background due to Drell-Yan processes (including $Z + \text{jets}$ production) where a jet provides a third genuine (non-prompt) lepton or a hadron misidentified as a lepton is evaluated from studies of isolated tracks, separately for samples enriched in heavy- and light-flavored jets. This background decreases rapidly to negligible levels for $E_T^{miss} > 50\,\text{GeV}$. The main backgrounds for $E_T^{miss} > 50\,\text{GeV}$ are from diboson and $t\bar{t}$ production and are estimated from the simulation with corrections and cross-checks as described below. Small backgrounds from rare SM processes such as ZZ, $t\bar{t}Z$, $t\bar{t}W$, and triboson production are estimated from simulation with a 50% systematic uncertainty based on NLO cross section calculations.

3.1.1 Background due to WZ production

The three-lepton analysis relies on E_T^{miss} and M_T to discriminate between signal and background. The largest irreducible background is from WZ production. It is therefore important that the E_T^{miss} and M_T distributions be well modeled in the WZ event simulation. For our study based on the 2011 data [8], we used the hadronic-recoil method, which is a generalization of the Z-recoil method used in the CMS measurements of the W and Z cross sections [36], to correct the E_T^{miss} distribution in simulated WZ events. In 2012, the rate of pileup interactions has

increased. We therefore developed a second method, described below, designed to specifically account for jet activity and pileup. We average the results of these complementary methods to correct the WZ simulation.

In the new method, we subdivide the $E_{\mathrm{T}}^{\mathrm{miss}}$ distribution as a function of the number of vertices and H_{T} in the event. A large number of vertices in an event corresponds to large pileup, which causes extraneous reconstruction of energy, thus worsening the $E_{\mathrm{T}}^{\mathrm{miss}}$ resolution. Larger H_{T} corresponds to a higher jet activity, which again leads to worsened $E_{\mathrm{T}}^{\mathrm{miss}}$ resolution as a consequence of the mis-reconstruction of jets.

We model the $E_{\mathrm{T}}^{\mathrm{miss}}$ distribution as a sum of Rayleigh distributions given by

$$p(E_{\mathrm{T}}^{\mathrm{miss}}) = \sum_{ij} W_{ij} \frac{E_{\mathrm{T}}^{\mathrm{miss}}}{\sigma_{ij}^2} e^{-E_{\mathrm{T}}^{\mathrm{miss}2}/2\sigma_{ij}^2}, \tag{3}$$

where i represents the number of vertices in the event, j the H_T bin, and W_{ij} the fraction of events in the bin. In this equation, σ_{ij} characterize the $E_{\mathrm{T}}^{\mathrm{miss}}$ resolution in both data and the simulation. We then adjust the $E_{\mathrm{T}}^{\mathrm{miss}}$ resolution in simulation on an event-by-event basis such that the coefficients match those found for data. The magnitude of the correction varies from a few percent to as high as 30%. To obtain a systematic uncertainty for this procedure, we vary the level of smearing and then determine the migration between different $E_{\mathrm{T}}^{\mathrm{miss}}$ and M_{T} bins in the WZ simulation sample. We find the WZ background uncertainty to be 25%.

3.1.2 Background due to fake and non-prompt leptons

Fake and non-prompt lepton backgrounds arise from $\mathrm{t\bar{t}}$, $\mathrm{Z}+\mathrm{jets}$, and $\mathrm{WW}+\mathrm{jets}$ events that have two genuine isolated prompt leptons. The third lepton can be a non-prompt lepton from a heavy-flavor decay that is classified as being prompt or a hadron from a jet misidentified as a lepton. This background is estimated using auxiliary data samples. The probability for a non-prompt lepton to satisfy the isolation requirement ($I_{\mathrm{rel}} < 0.15$) is measured in a data sample enriched with QCD dijet events, and varies as a function of lepton p_{T}. Alternatively, the isolation probability is studied using Z-boson and $\mathrm{t\bar{t}}$-enriched data samples. These probabilities, applied to the three-lepton events with the isolation requirement on one of the leptons inverted, are used to estimate background due to such non-prompt leptons.

Another background estimated with data occurs when a Z boson decay is accompanied by an initial- or final-state radiation photon that converts internally, leading to a reconstructed three-lepton final state when the conversion is highly asymmetric [9]. To address this background, we measure the rate of $\mathrm{Z} \to \ell^+\ell^-\gamma$ and $\mathrm{Z} \to \ell^+\ell^-\ell^\pm$ events in an off-peak control region defined by $|M_{\ell\ell} - M_{\mathrm{Z}}| > 15$ GeV. The background estimate is obtained by applying the ratio of these rates to events with two leptons and a photon in the signal region. External conversions are strongly suppressed by our electron object selection.

The systematic uncertainty for backgrounds with mis-identified or non-prompt leptons obtained from data-driven methods is estimated from the difference between the predicted and true yields when the methods are applied to simulation.

3.2 Three-lepton search results

Figure 4 shows the distribution of M_{T} versus $M_{\ell\ell}$ for events with an ee or $\mu\mu$ OSSF pair, where the third lepton is either an electron or muon. The dashed lines indicate six two-dimensional search regions in the M_{T}-$M_{\ell\ell}$ plane. The corresponding $E_{\mathrm{T}}^{\mathrm{miss}}$ distributions for the six regions are shown in Fig. 5. The latter results are compared to the SM expectations. The uncertainties

on the data points are Poissonian, including those for bins with zero entries. Table 1 lists the results as a function of $E_{\mathrm{T}}^{\mathrm{miss}}$, M_{T} and $M_{\ell\ell}$. Figures 6, 7, and Table 2 show the corresponding results for eeμ and e$\mu\mu$ events without an OSSF pair. Figures 8, 9 and Table 3 show the results for events with a same-sign ee , eμ, or $\mu\mu$ pair and one hadronic τ lepton. Figures 10, 11 and Table 4 show the results for events with an opposite-sign eμ pair and one hadronic τ lepton.

In Section 8, we present an interpretation of the results of this search for several models of chargino-neutralino production.

4 Search in the four-lepton final state

As mentioned in the introduction, we interpret our four-lepton final state results in the context of a GMSB model, in combination with the results from the final state with two leptons plus at least two jets, which is presented in Section 6. This situation motivates the use of four-lepton channels with at least one OSSF pair that is consistent with a Z decay. The data are binned in intervals of $E_{\mathrm{T}}^{\mathrm{miss}}$ in order to discriminate between signal and background.

We use the same object selection as for the three-lepton final state, requiring exactly four leptons (electrons, muons, and at most one hadronically decaying tau lepton). We require that there be an ee or $\mu\mu$ OSSF pair with an invariant mass within 15 GeV of the Z boson mass. The background determination methods are also the same as described for the three-lepton final state. The primary background, from ZZ production, is thus estimated from simulation, with corrections applied to the predicted $E_{\mathrm{T}}^{\mathrm{miss}}$ spectrum as described in Section 3.1.1. Background due to hadrons that are misreconstructed as leptons or due to non-prompt leptons is evaluated using control samples in the data.

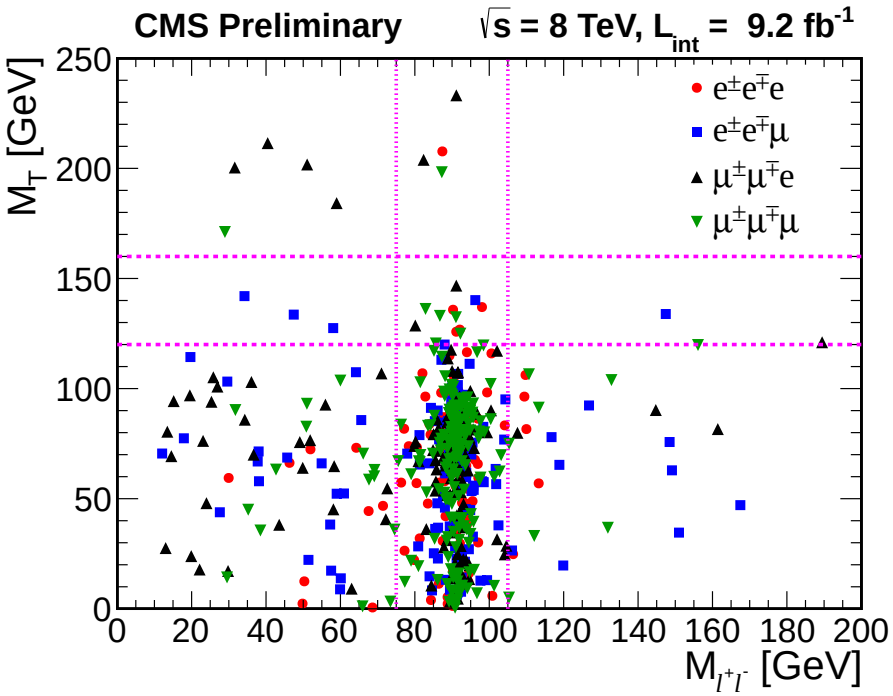

Figure 4: M_{T} versus $M_{\ell\ell}$ for three-lepton events with an ee or $\mu\mu$ OSSF dilepton pair, where the third lepton is either an electron or a muon.

Table 1: SM expectations and observations for events with an ee or $\mu\mu$ OSSF pair, where the third lepton is either an electron or muon.

M_{T} (GeV)	$E_{\mathrm{T}}^{\mathrm{miss}}$ (GeV)	$M_{\ell\ell} < 75$ GeV		75 GeV $< M_{\ell\ell} <$ 105 GeV		$M_{\ell\ell} > 105$ GeV	
		total bkg	observed	total bkg	observed	total bkg	observed
> 160	50 – 100	2.1±0.5	4	3.3±0.5	3	1.2±0.7	0
	100 – 150	1.7±0.4	0	1.8±0.2	1	1.1±0.7	1
	150 – 200	0.8±0.3	1	0.63±0.16	1	0.26±0.18	0
	> 200	0.25±0.20	0	0.58±0.19	1	0.18±0.14	0
120 – 160	50 – 100	3.5±0.5	3	10.0±0.6	11	1.30±0.19	0
	100 – 150	1.1±0.3	0	1.5±0.2	0	0.17±0.05	2
	150 – 200	0.15±0.16	0	0.4±0.4	1	0.12±0.10	0
	> 200	0.11±0.05	0	0.17±0.10	1	0.08±0.09	0
0 – 120	50 – 100	53±5	63	382±15	377	19.0±1.7	22
	100 – 150	6.6±1.0	5	63±3	61	4.0±0.6	6
	150 – 200	1.4±0.3	1	16.0±0.9	13	0.9±0.3	2
	> 200	0.54±0.17	1	9.5±0.6	3	0.43±0.08	2

Table 2: SM expectations and observations for eeμ and e$\mu\mu$ events without an OSSF pair or a hadronic τ lepton candidate.

M_{T} (GeV)	$E_{\mathrm{T}}^{\mathrm{miss}}$ (GeV)	$M_{\ell\ell} < 100$ GeV		$M_{\ell\ell} > 100$ GeV	
		total bkg	observed	total bkg	observed
> 160	50 – 100	1.0±0.3	1	0.5±0.8	0
	100 – 150	0.6±0.3	0	0.16±0.14	0
	150 – 200	0.16±0.17	0	0.03±0.07	0
	> 200	0.08±0.05	0	0.07±0.06	0
120 – 160	50 – 100	2.0±0.6	1	0.11±0.03	1
	100 – 150	0.5±0.6	1	0.06±0.07	0
	150 – 200	0.08±0.07	1	0.00021±0.00019	0
	> 200	0.013±0.008	0	0.004±0.005	0
0 – 120	50 – 100	12.0±2.4	12	0.61±0.16	0
	100 – 150	2.5±0.6	2	0.07±0.02	0
	150 – 200	0.16±0.06	0	0.08±0.08	0
	> 200	0.24±0.22	0	0.00021±0.00017	0

Table 3: SM expectations and observations for events with a same-sign ee , eμ, or $\mu\mu$ pair and a hadronic τ candidate.

M_{T} (GeV)	$E_{\mathrm{T}}^{\mathrm{miss}}$ (GeV)	$M_{\ell\ell} < 100$ GeV		$M_{\ell\ell} > 100$ GeV	
		total bkg	observed	total bkg	observed
> 160	50 – 100	1.8±0.5	1	0.22±0.13	1
	100 – 150	0.8±0.3	0	0.21±0.15	1
	150 – 200	0.30±0.17	0	0.07±0.04	0
	> 200	0.22±0.12	2	0.012±0.009	0
120 – 160	50 – 100	3.1±0.8	3	0.056±0.033	0
	100 – 150	0.54±0.21	1	0.013±0.010	0
	150 – 200	0.03±0.02	0	0±0	0
	> 200	0.032±0.024	0	0.0065±0.0064	0
0 – 120	50 – 100	33±6	25	1.3±0.4	1
	100 – 150	3.9±1.0	0	0.29±0.11	0
	150 – 200	0.8±0.3	0	0.04±0.03	0
	> 200	0.31±0.14	0	0.027±0.024	0

Table 4: SM expectations and observations for events with an opposite-sign eμ pair and a hadronic τ candidate.

M_{T} (GeV)	$E_{\mathrm{T}}^{\mathrm{miss}}$ (GeV)	$M_{\ell\ell} < 100$ GeV		$M_{\ell\ell} > 100$ GeV	
		total bkg	observed	total bkg	observed
> 160	50 – 100	6.7±3.2	9	1.9±0.9	0
	100 – 150	5.2±3.2	8	1.2±0.9	1
	150 – 200	0.4±0.3	1	0.3±0.4	1
	> 200	0.4±0.3	1	0.055±0.019	0
120 – 160	50 – 100	18±7	21	3.4±1.5	1
	100 – 150	6.7±3.6	6	0.54±0.41	1
	150 – 200	0.34±0.25	1	6.6e-05±7.5e-05	0
	> 200	0.025±0.012	1	0.23±0.24	0
0 – 120	50 – 100	114±37	124	12±5	12
	100 – 150	22±9	28	2.4±1.0	3
	150 – 200	4.3±2.1	3	1.1±0.8	0
	> 200	0.25±0.10	1	0.10±0.07	0

Table 5 summarizes the results. We consider events with exactly one OSSF pair and no hadronic tau candidate, with exactly one OSSF pair and one hadronic tau candidate, and with exactly two OSSF pairs and no hadronic tau candidate. Figure 12 presents the distribution of $E_{\mathrm{T}}^{\mathrm{miss}}$ versus $M_{\ell\ell}$ for events without a tau candidate. For events with two OSSF pairs, we choose the pair with mass closest to the Z boson mass.

The interpretation of the four-lepton results is presented in Section 8.

5 Search in the same-sign two-lepton final state

Three-lepton final states are not sensitive to the chargino-neutralino pair-production processes of Fig. 1 if one of the leptons is unidentified, not isolated, or outside the acceptance of the analysis. For small mass differences between the SUSY particle states in Fig. 1, one of the leptons might be too soft to be included in the analysis. Some of these otherwise-rejected events can be recovered by requiring only two leptons, which should, however, be of the same sign (SS) to suppress the overwhelming background from OSSF pairs.

We therefore perform a search for events with two SS leptons. We require that events contain either an SS ee, eμ, or $\mu\mu$ pair, where the e and μ candidates are required to satisfy $p_{\mathrm{T}} > 20\,\mathrm{GeV}$ and $|\eta| < 2.4$. To better reject background, we tighten the e (μ) isolation requirement to $I_{\mathrm{rel}} < 0.09\ (0.10)$.

Background from processes such as WZ and $\mathrm{t\bar{t}Z}$ production is reduced by rejecting events that, after applying looser e and μ selection criteria, contain an OSSF pair within 15 GeV of the Z

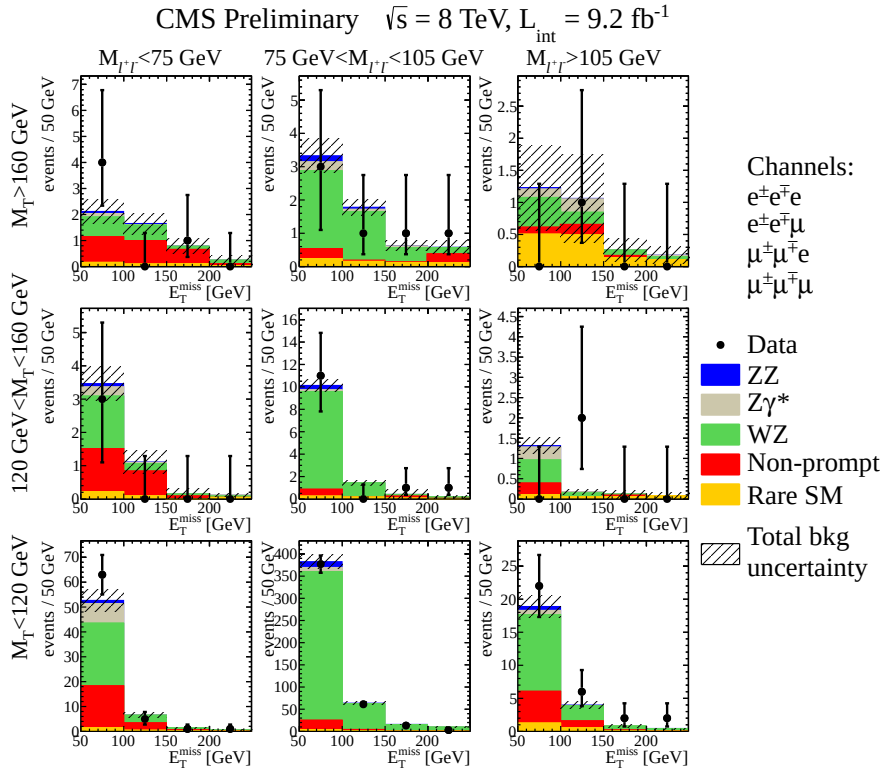

Figure 5: Observed $E_{\mathrm{T}}^{\mathrm{miss}}$ distribution for three-lepton data events with an ee or $\mu\mu$ OSSF dilepton pair, where the third lepton is either an electron or a muon. SM expectations are also shown. "Rare SM" refers to standard model processes such as ZZ, $\mathrm{t\bar{t}Z}$, $\mathrm{t\bar{t}W}$, and triboson production.

boson mass.

We evaluate the background from WZ events using simulation and assign a 20% systematic uncertainty, which accounts for the difference between the observed and simulated yields in a WZ-event-enriched data control sample obtained by inverting the Z veto. A second remaining background is due to events with a genuine lepton from heavy-flavor decay or a misidentified hadron (mainly from $t\bar{t}$ events). We evaluate this background by determining the probability for a loosely identified e or μ to satisfy the selection criteria in a background-enriched control region [34]. We assign a 50% systematic uncertainty to this background. A third background is from events with two opposite-sign leptons, in which one of the leptons is an electron with a badly reconstructed charge due to severe bremsstrahlung. To evaluate this background, we select opposite-sign events that pass the full kinematic selection, weighted by the probability of electron-charge misassignment (obtained from $Z \to ee$ events). Finally, background from rare SM processes such as those described in Section 3.1 is estimated from simulation, with a 50% uncertainty.

The distribution of $E_{\mathrm{T}}^{\mathrm{miss}}$ versus H_{T} for the SS events is shown in Fig. 13. The region with $E_{\mathrm{T}}^{\mathrm{miss}} > 200\,\mathrm{GeV}$ defines a signal region. The region with $120 < E_{\mathrm{T}}^{\mathrm{miss}} < 200\,\mathrm{GeV}$ defines a control region. The subset of events in the control region with $N_{jets} \leq 2$ and $N_{bjets} = 0$ defines a second signal region. Table 6 shows the observed yields and the SM expectations for the two signal regions. The table also shows the results after events with a third lepton that satisfy the criteria of Section 3 are excluded in order to facilitate combination with those results. This table has been updated since the original release of this Analysis Summary on 2012/11/27 to reflect a correction in the fake background estimation.

The interpretation of the results is presented in Section 8.

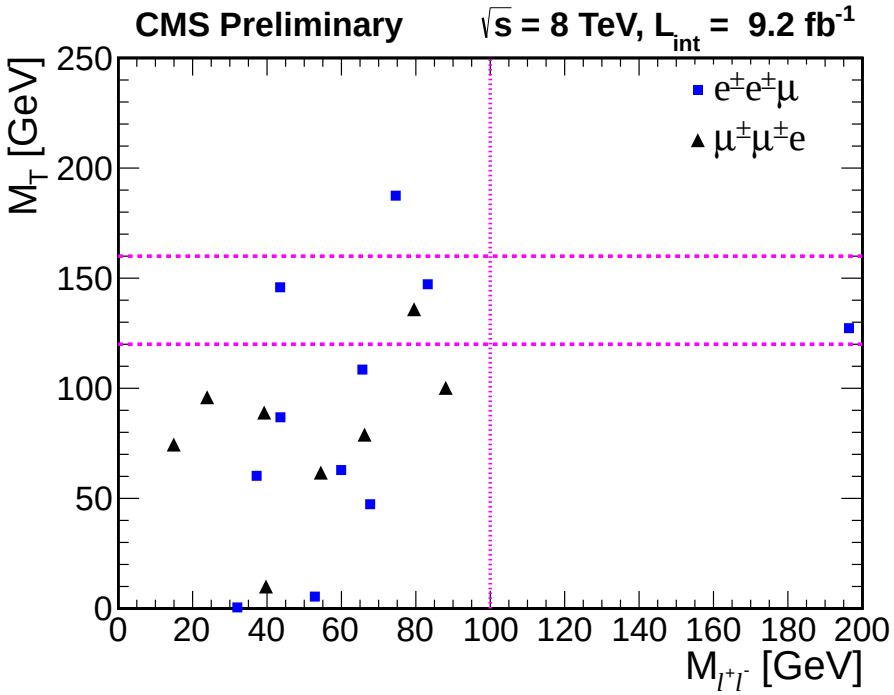

Figure 6: M_{T} versus $M_{\ell\ell}$ for three-lepton events without an OSSF dilepton pair or a hadronic τ lepton candidate.

6 Search in the WZ/ZZ + E_T^{miss} final state with two leptons and two jets

The three- and four-lepton searches described above are also sensitive to the processes illustrated in Fig. 2, with two on-shell vector bosons. In this section, we describe a search for events with two leptons and at least two jets, which extends sensitivity to these processes. Specifically, we select events in which a Z boson decays to either an ee or $\mu\mu$ pair, while a W boson or another Z boson decays to two jets. The object selection and background determination procedures are based on those presented in Ref. [37]; both leptons must have $p_T > 20$ GeV and an invariant mass consistent with the Z boson to within 10 GeV. At least two jets with $p_T > 30$ GeV are required. Events with a third lepton are rejected in order to reduce the background from WZ events.

Following the lepton and jet selection, the dominant background is from Z + jets events. This background is strongly suppressed by adding the requirement of large E_T^{miss}, leaving $t\bar{t}$ production as the dominant background. The $t\bar{t}$ background is reduced by a factor of 10 by the

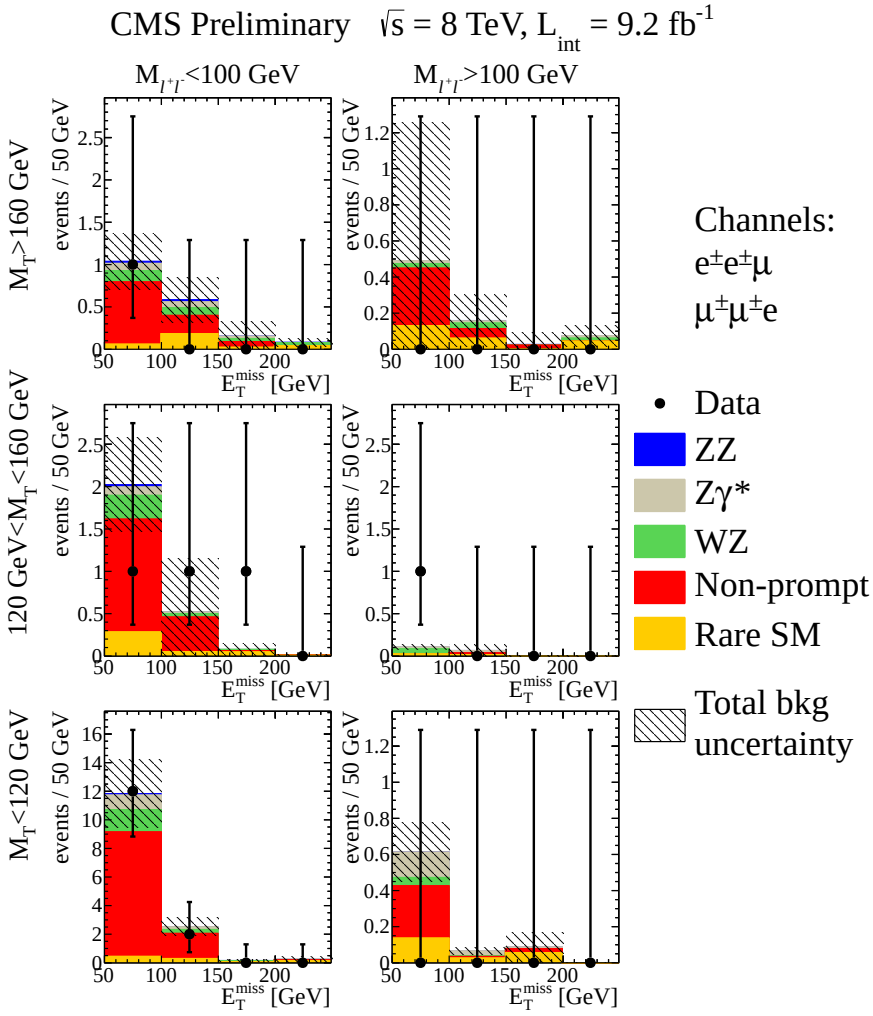

Figure 7: Observed E_T^{miss} distribution for the data events without an OSSF dilepton pair or a hadronic τ lepton. SM expectations are also shown."Rare SM" refers to standard model processes such as ZZ, $t\bar{t}Z$, $t\bar{t}W$, and triboson production.

veto on events with b jets mentioned in Section 2. Background from $t\bar{t}$ and $Z+$jets events is reduced further by requiring the dijet mass M_{jj} to be consistent with a W or Z boson, namely $70\,\text{GeV} < M_{jj} < 110\,\text{GeV}$.

For the remaining background from $Z+$jets events, significant $E_{\text{T}}^{\text{miss}}$ arises primarily because of the mismeasurement of jet p_{T}. We evaluate the remaining $Z+$jets background using a sample of $\gamma+$jets events as described in Ref. [37], accounting for the different kinematic properties of the events in the control and signal samples.

The remaining background with uncorrelated flavor is dominated by $t\bar{t}$ events, but also includes events with WW, single-top, and $\tau\tau$ production. This background is characterized by equal rates of ee $+\,\mu\mu$ versus eμ events and so is denoted "flavor symmetric." To evaluate the flavor-symmetric background, we use an eμ event sample, as described Ref. [37]. SM backgrounds from events with WZ and ZZ production are estimated from simulation and assigned uncertainties based on comparisons with data in control samples with exactly three leptons (WZ control sample) and exactly four leptons (ZZ control sample), and at least two jets. Backgrounds from rare SM processes with $t\bar{t}Z$, ZZZ, ZZW, and ZWW production are assessed from simulation with a 50% uncertainty.

The results are presented in Table 7, which also indicates the signal regions used for the search. Figure 14 displays the same information graphically. The interpretation of the results is presented in Section 8.

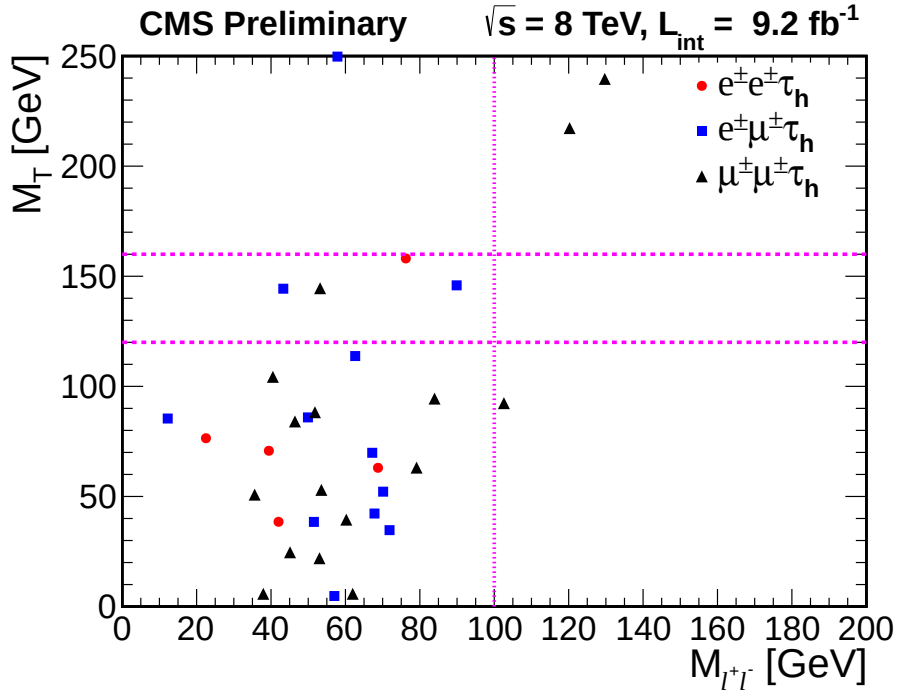

Figure 8: M_{T} versus $M_{\ell\ell}$ for the three-lepton data events containing a same-sign ee, eμ, or $\mu\mu$ pair and a hadronic τ lepton candidate.

7 Search with non-resonant opposite-sign dileptons

Finally, we present a search for events with an oppositely charged ee, eμ, or $\mu\mu$ pair, in which the ee and $\mu\mu$ pairs are required to be inconsistent with Z boson decay. The search is sensitive to the processes shown in Fig. 3.

Both leptons must have $p_T > 20\,\text{GeV}$. The ee or $\mu\mu$ invariant mass must differ from the Z boson mass by at least 15 GeV. Events are required to have $E_T^{\text{miss}} > 60\,\text{GeV}$.

The remaining background, which is mostly composed of events with $t\bar{t}$ and WW production, is reduced using a variable called $M_{CT\perp}$ [38]. This variable is closely related to another variable known as M_{CT} [39], which is suitable in situations when two identical particles that each decay to a visible particle and an LSP are produced at rest in the laboratory frame. In such situations, M_{CT} has a maximum value that depends only on the masses of the parent (P) and invisible-child (C):

$$M_{CT}^{\max} = \frac{M_P^2 - M_C^2}{M_P}. \tag{4}$$

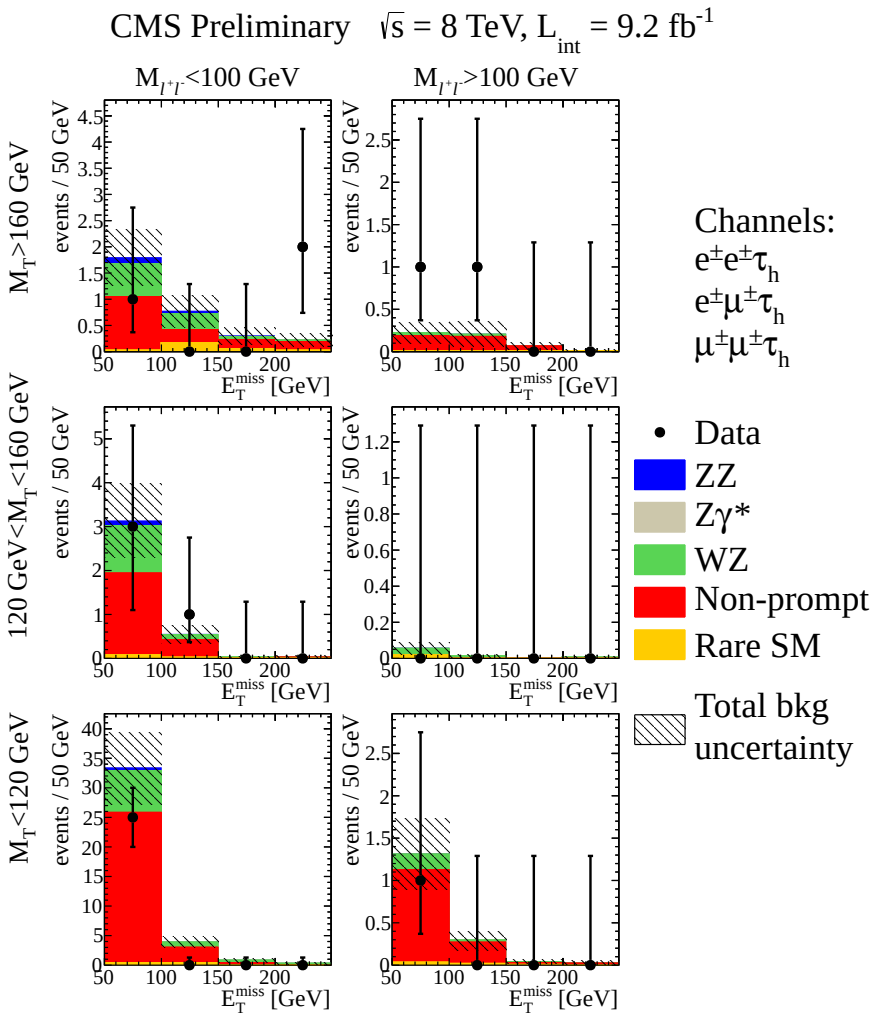

Figure 9: Observed E_T^{miss} distribution for the data events with a same-sign ee, eμ, or $\mu\mu$ pair and a hadronic τ lepton candidate. SM expectations are also shown. "Rare SM" refers to standard model processes such as ZZ, $t\bar{t}Z$, $t\bar{t}W$, and triboson production.

The $M_{CT\perp}$ variable is an extension of M_{CT} . The momentum of the system against which the visible particles recoil is calculated, and the visible particle momenta are then projected onto the plane perpendicular to the recoil direction. In practice, the recoil direction is determined by taking the negative of the E_T^{miss} vector and and subtracting the visible particle momenta. The $M_{CT\perp}$ variable preserves the endpoint of Eq. (4) for situations in which the pair-produced particles "P" are not produced at rest.

In events where both leptons and E_T^{miss} originate from W bosons, $M_P = M_W$ and $M_C = M_\nu$, and the $M_{CT\perp}$ variable is expected to exhibit a kinematic limit at the W boson mass. To allow for measurement resolution, we require $M_{CT\perp} > 100\,\text{GeV}$.

The SM background is estimated using templates describing the $M_{CT\perp}$ shapes for the different background categories. First, an $M_{CT\perp}$ template is defined for each background category using either a control sample in data or simulation. Then a sum of these templates is fit to a low $M_{CT\perp}$ control region of the data, $5 < M_{CT\perp} < 100\,\text{GeV}$, where background is expected to dominate. The fit determines the overall normalization for each template. The predictions of the normalized templates in the high $M_{CT\perp}$ region provide the background estimates in the signal region.

The template shape for backgrounds containing top quarks is estimated from a control sample containing one or more identified b jet. We evaluate the average b-jet tagging efficiency by measuring the ratio of the number of events with two identified b jets to the number with one identified b jet. After applying a correction factor of 6% obtained from simulation, this efficiency is used to predict the number of top quark events without an identified b jet in data. A 6% systematic uncertainty is assigned to the efficiency, which leads to a 12% systematic uncertainty for the top background normalization constraint.

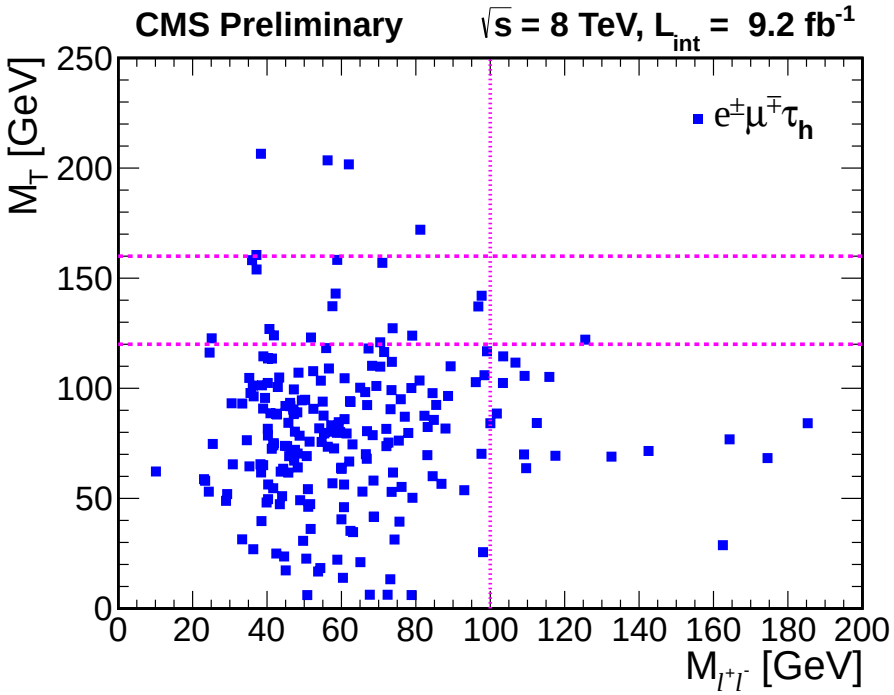

Figure 10: M_T versus $M_{\ell\ell}$ for the three-lepton data events containing an opposite-sign, opposite-flavor eμ pair and a hadronic τ lepton candidate.

A single template is used for all diboson categories, including events with WW, WZ, and ZZ production. This template is derived from Monte Carlo simulation. The event simulation is validated by verifying the agreement between data and simulation in the high-$M_{CT\perp}$, on-Z region, where the ZZ background is dominant. For $M_{CT\perp} > 100\,\text{GeV}$, 46.6 $\pm$1.8 events are predicted by the simulation, while 50 events are observed.

Similarly, a template for backgrounds with two leptons from an off-shell Z boson with E_T^{miss} from misreconstructed jets is obtained from simulation. We examine the low-$M_{CT\perp}$ on-Z region ($M_{CT\perp} < 100\,\text{GeV}$ and $|M_{\ell\ell} - M_Z| < 15$ GeV), where this background is expected to dominate, to verify that the shape of this background is well modeled by the simulation.

Because backgrounds from Z and ZZ processes only contribute to the ee and $\mu\mu$ final states, we derive separate templates and background estimates for same-flavor and opposite-flavor events. The results are presented in Table 8 and in Figs. 15(a) and (b). The interpretation of the results is given in Section 8.

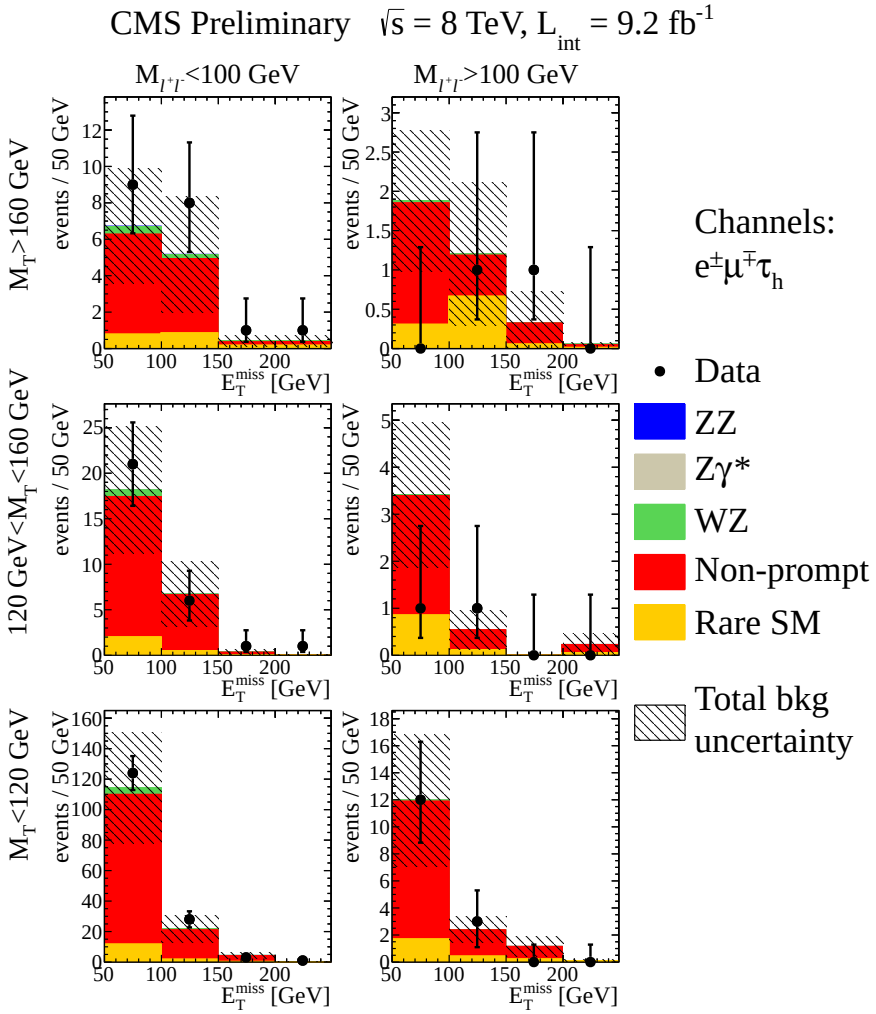

Figure 11: Observed E_T^{miss} distribution for the data events with an opposite-sign, opposite-flavor eμ pair and a hadronic τ lepton candidate. SM expectations are also shown. "Rare SM" refers to standard model processes such as ZZ, $t\bar{t}Z$, $t\bar{t}W$, and triboson production.

Table 5: Expected SM backgrounds and observed yields for exclusive channels of four-lepton final states. All categories have four leptons including an OSSF pair consistent with a Z boson. The three sections refer, respectively, to events with one OSSF pair and no hadronic τ candidate, one OSSF and one hadronic τ candidate, and two OSSF pairs and no hadronic τ candidate.

$E_{\mathrm{T}}^{\mathrm{miss}}$ (GeV)	Observed	Total Bkg
1 OSSF, 0 τ		
0–30	0	$3.94 \pm 0.32 \pm 1.32$
30–50	1	$0.71 \pm 0.10 \pm 0.18$
50–100	1	$0.74 \pm 0.09 \pm 0.17$
> 100	0	$0.36 \pm 0.04 \pm 0.12$
1 OSSF, 1 τ		
0–30	13	$11.33 \pm 0.51 \pm 2.44$
30–50	4	$5.50 \pm 0.20 \pm 0.73$
50–100	6	$4.93 \pm 0.17 \pm 0.55$
> 100	1	$1.62 \pm 0.09 \pm 0.19$
2 OSSF, 0 τ		
0–30	69	$68.52 \pm 1.04 \pm 20.18$
30–50	9	$9.31 \pm 0.32 \pm 3.08$
50–100	1	$1.67 \pm 0.14 \pm 0.56$
> 100	0	$0.31 \pm 0.03 \pm 0.12$

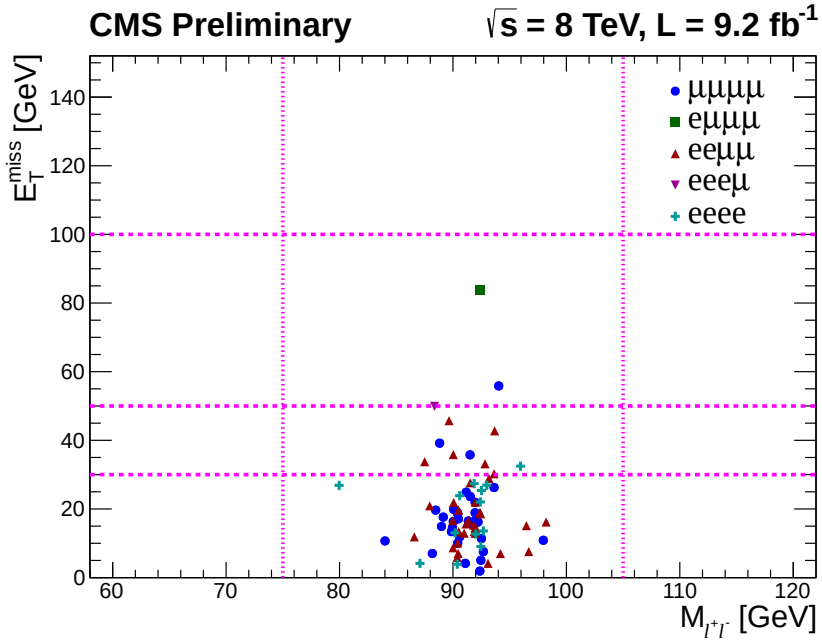

Figure 12: $E_{\mathrm{T}}^{\mathrm{miss}}$ versus $M_{\ell\ell}$ for four-lepton data events with an on-Z OSSF pair and no hadronic τ lepton candidate. The legend indicates the flavor breakdown of events.

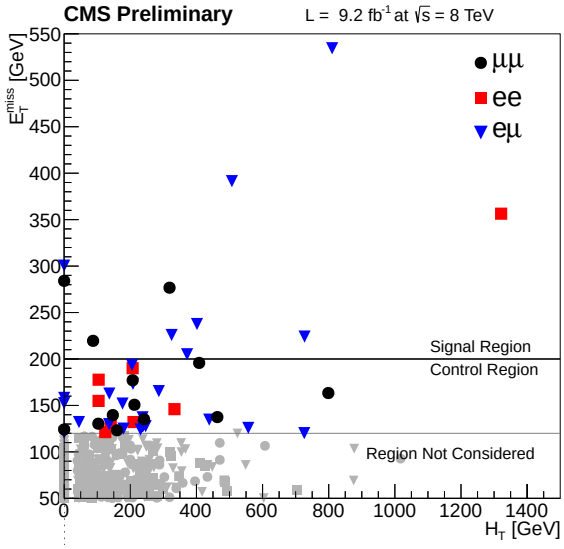

Figure 13: $E_{\mathrm{T}}^{\mathrm{miss}}$ versus H_{T} for same-sign dilepton candidate events. Only the $E_{\mathrm{T}}^{\mathrm{miss}} > 120\,\mathrm{GeV}$ region is considered in this analysis.

Table 6: Summary of background predictions and observed yields for search regions: $120 < E_{\mathrm{T}}^{\mathrm{miss}} < 200$ GeV, $N_{jets} \leq 2$ and $N_{bjets} = 0$, and $E_{\mathrm{T}}^{\mathrm{miss}} > 200$ GeV, with and without third lepton veto applied (including taus). Uncertainties include statistical and systematic contributions. This table has been revised since its original release to reflect a correction in the fake background estimation.

	$120 < E_{\mathrm{T}}^{\mathrm{miss}} < 200$ GeV $N_{jets} \leq 2$, $N_{bjets} = 0$	$120 < E_{\mathrm{T}}^{\mathrm{miss}} < 200$ GeV $N_{jets} \leq 2$, $N_{bjets} = 0$ 3^{rd} lepton veto	$E_{\mathrm{T}}^{\mathrm{miss}} > 200$ GeV	$E_{\mathrm{T}}^{\mathrm{miss}} > 200$ GeV 3^{rd} lepton veto
Double Fakes	0.05 ± 0.06	0.03 ± 0.04	< 0.02	0.01 ± 0.02
Single Fakes	8.6 ± 4.5	7.3 ± 3.8	3.5 ± 1.9	2.8 ± 1.6
Charge MisID	0.42 ± 0.03	0.40 ± 0.03	0.14 ± 0.01	0.13 ± 0.01
Rare SM	5.0 ± 2.6	4.3 ± 2.3	4.7 ± 2.5	4.0 ± 2.2
WZ Prod.	8.3 ± 1.6	6.2 ± 1.2	2.7 ± 0.5	2.0 ± 0.4
Total Bkg	22.4 ± 5.4	18.2 ± 4.6	11.0 ± 3.2	8.9 ± 2.7
Data	14	11	11	7

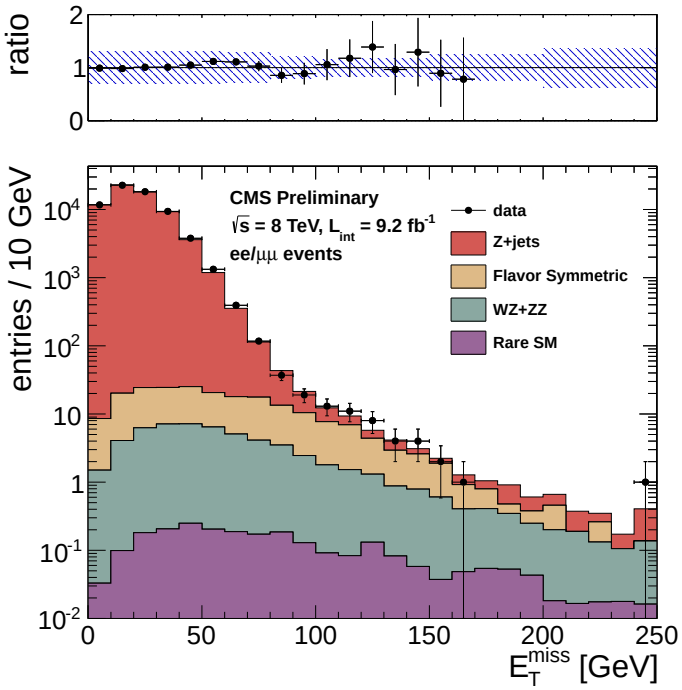

Figure 14: Results of the Z + dijet analysis. The observed E_T^{miss} distribution (black points) is compared with the sum of the predicted E_T^{miss} distributions from the Z + jets, flavor-symmetric, sum of WZ and ZZ, and rare SM backgrounds. The ratio of observed to predicted yields in each bin is indicated in the upper plot. The error bars indicate the statistical uncertainty in the data and the shaded band indicates the total background uncertainty. "Rare SM" refers to standard model processes such as ZZ, $t\bar{t}Z$, $t\bar{t}W$, and triboson production.

Table 7: Summary of results in the Z + dijet analysis. The total background is the sum of the Z + jets background predicted from the E_T^{miss} templates method (Z + jets bkg), the flavor-symmetric (FS) background predicted from eμ events, and the WZ, ZZ, and rare SM backgrounds predicted from MC. All uncertainties include both the statistical and systematic components.

	E_T^{miss} 0–30 GeV	E_T^{miss} 30–60 GeV	E_T^{miss} 60–80 GeV	E_T^{miss} 80–100 GeV
Z + jets bkg	52823 ± 15847	14015 ± 4205	433 ± 130	40.9 ± 12.4
FS bkg	41.3 ± 7.2	49.5 ± 8.6	26.4 ± 4.7	17.9 ± 3.3
WZ bkg	9.5 ± 6.6	15.9 ± 11.2	6.6 ± 4.7	3.9 ± 2.7
ZZ bkg	2.1 ± 1.0	4.1 ± 2.1	2.2 ± 1.1	1.8 ± 0.9
rare SM bkg	0.3 ± 0.2	0.7 ± 0.3	0.4 ± 0.2	0.3 ± 0.2
total bkg	52876 ± 15847	14085 ± 4205	468 ± 130	64.7 ± 13.2
data	52485	14476	510	56
	E_T^{miss} 100–120 GeV	E_T^{miss} 120–150 GeV	E_T^{miss} 150–200 GeV	$E_T^{miss} > 200$ GeV
Z + jets bkg	7.0 ± 2.2	3.1 ± 0.9	1.6 ± 0.5	0.8 ± 0.3
FS bkg	11.3 ± 2.2	6.9 ± 1.5	2.4 ± 1.1	0.4 ± 0.3
WZ bkg	2.1 ± 1.5	1.6 ± 1.1	1.0 ± 0.7	0.5 ± 0.5
ZZ bkg	1.0 ± 0.5	1.1 ± 0.6	0.8 ± 0.4	0.7 ± 0.7
rare SM bkg	0.2 ± 0.1	0.3 ± 0.1	0.2 ± 0.1	0.2 ± 0.2
total bkg	21.7 ± 3.5	13.0 ± 2.2	6.1 ± 1.5	2.5 ± 0.9
data	24	16	3	1

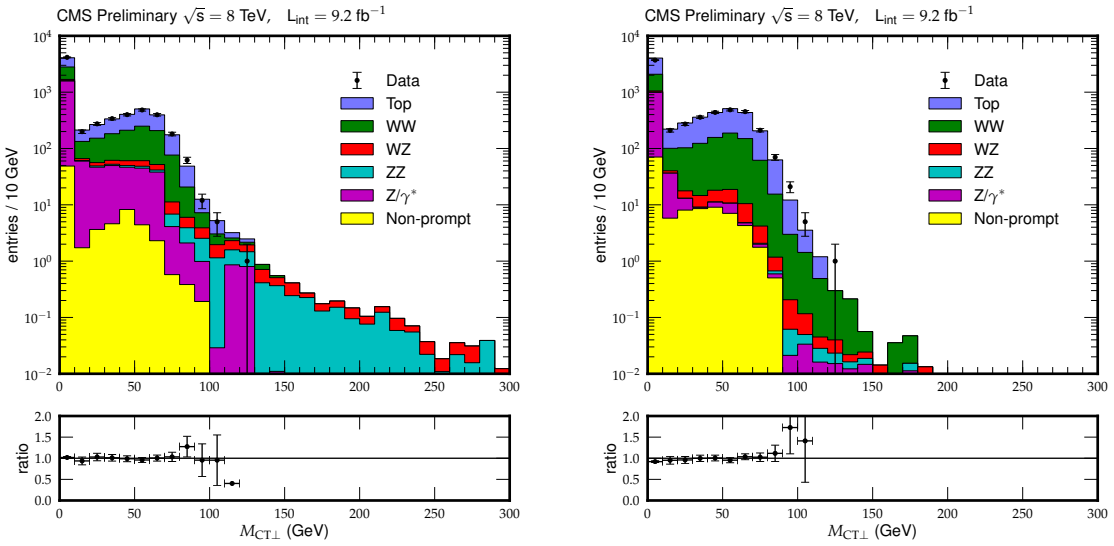

(a) same-flavor (b) opposite-flavor

Figure 15: The $M_{CT\perp}$ distributions in data (black points) and background prediction (filled histogram) for a (a) same-flavor and (b) opposite-flavor dileptons. The large event yield in the lowest bin is an expected feature of the $M_{CT\perp}$ variable, as a large region of phase space yields $M_{CT\perp} = 0$. The small, lower plots show the ratio of the data to the fit results, with statistical uncertainties.

Table 8: Results from the fit to data in the low $M_{CT\perp}$ control region and extrapolation to the high $M_{CT\perp}$ signal region in the same- and opposite-flavor channels. Since the contributions of the individual backgrounds in the low $M_{CT\perp}$ region are derived from a fit to data, they by definition add to the number of events in that region in data.

	Opposite Flavor		Same Flavor	
	$5 < M_{CT\perp} < 100\,\text{GeV}$	$M_{CT\perp} > 100\,\text{GeV}$	$5 < M_{CT\perp} < 100\,\text{GeV}$	$M_{CT\perp} > 100\,\text{GeV}$
Top	1660 ± 175	2.8 ± 1.0	1133 ± 130	3.1 ± 1.1
WW	796 ± 204	2.3 ± 1.7	883 ± 160	1.8 ± 0.8
WZ	38 ± 10	0.1 ± 0.1	64 ± 12	3.0 ± 1.4
ZZ	0.8 ± 0.2	0.1 ± 0.1	24 ± 4	4.6 ± 2.1
DY	59 ± 24	0.1 ± 0.4	305 ± 64	1.7 ± 1.2
W	47 ± 116	0.0 ± 0.0	27 ± 101	0.0 ± 0.0
Total	see caption	5.4 ± 2.1	see caption	14.2 ± 4.5
Data	2604	6	2438	6

8 Interpretations of the searches

In this section, we present the interpretation of our results. In all the search channels, the observations agree with the expected background. We calculate upper limits on the cross sections for the pair production of charginos, neutralinos, and sleptons.

The 95% confidence level (CL) upper limits are computed using the CL_s method [40–42]. For each point in the signal parameter space, we omit from consideration channels that make negligible contributions to the overall sensitivity. We use the NLO cross section from Ref. [19–21] to evaluate 95% CL exclusion curves and their one standard deviation (σ) uncertainty. In addition, we display the median expected exclusion limits.

8.1 Limits on SMS from the search with three leptons and from same-sign dilepton searches

Figure 16 displays the results of the three-lepton search. The figure depicts the 95% CL upper limit on the cross section times branching fraction in the $m_{\widetilde{\chi}_1^0}$ versus $m_{\widetilde{\chi}_2^0}$ ($= m_{\widetilde{\chi}_1^\pm}$) plane in the flavor-democratic scenario described in the Introduction. The corresponding results for the combination of the SS dilepton and three-lepton searches are shown in Fig. 17 for two values of $x_{\widetilde{\ell}}$ (0.05 and 0.95).

Figure 18 presents the corresponding limits for the τ-enriched scenario and Fig. 19 for the τ-dominated scenario. As the SS dilepton search does not have sensitivity for $x_{\widetilde{\ell}} = 0.50$, there is no limit curve for this search for Figures 16, 18(b), and 19. For the other limit curves in Figs. 17, 18 and 19, the increase in the combined mass limit from incorporation of the SS dilepton search takes place in the experimentally challenging region where the neutralinos have similar masses.

8.2 Limits on SMS with on-shell W and Z from $\mathrm{WZ} + E_{\mathrm{T}}^{\mathrm{miss}}$ and three-lepton analyses

To evaluate upper limits on the process of Fig. 2(a), we use the results of the $\mathrm{WZ/ZZ} + E_{\mathrm{T}}^{\mathrm{miss}}$ analysis together with the three-lepton analysis. Assuming 100% branching fractions of the chargino to $\mathrm{W} + \widetilde{\chi}_1^0$ and neutralino to $\mathrm{Z} + \widetilde{\chi}_1^0$, we calculate upper limits on the cross section for chargino-neutralino production times branching fractions into the $\mathrm{WZ} + E_{\mathrm{T}}^{\mathrm{miss}}$ final state as a function of the chargino and neutralino masses. Figure 20 displays the observed limits for the component analyses and the combination. The sensitivity of the three-lepton and $\mathrm{WZ/ZZ} + E_{\mathrm{T}}^{\mathrm{miss}}$ analyses are complementary, with the three-lepton results dominating the sensitivity in the region where the difference between the neutralino masses is small, and the $\mathrm{WZ/ZZ} + E_{\mathrm{T}}^{\mathrm{miss}}$ results dominating the sensitivity in the region where $m_{\widetilde{\chi}_2^0} = m_{\widetilde{\chi}_1^\pm}$ is large.

8.3 Limits on a Z-enriched GMSB model

We consider a gauge-mediated symmetry breaking (GMSB) Z-enriched higgsino model [8, 10, 11] because it has a large branching fraction to the $\mathrm{ZZ} + E_{\mathrm{T}}^{\mathrm{miss}}$ final state. The LSP in this model is an almost massless gravitino, the next-to-lightest SUSY particle is a Z-enriched higgsino $\widetilde{\chi}_1^0$, and the $\widetilde{\chi}_1^\pm$ is nearly degenerate in mass with the $\widetilde{\chi}_1^0$. We set the gaugino mass parameters M_1 and M_2 to $M_1 = M_2 = 1\,\mathrm{TeV}$ and the ratio of Higgs expectation values $\tan\beta$ to $\tan\beta = 2$. The results are presented as a function of the gaugino mass parameter μ, where $m_{\widetilde{\chi}_1^0} \approx m_{\widetilde{\chi}_2^0} \approx m_{\widetilde{\chi}_1^\pm} \approx \mu$ to within typical mass differences of a few GeV. The branching fraction to the $\mathrm{ZZ} + E_{\mathrm{T}}^{\mathrm{miss}}$ final state varies from 100% at $\mu = 130$ GeV to 85% at $\mu = 410$ GeV. We use the results of the

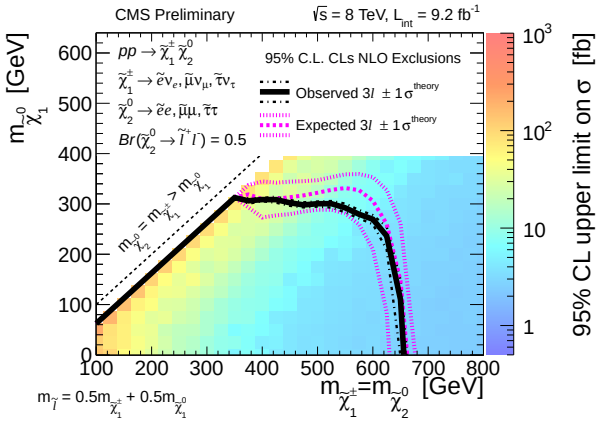

Figure 16: The shading in the $m_{\tilde{\chi}_1^0}$ versus $m_{\tilde{\chi}_2^0}$ ($= m_{\tilde{\chi}_1^\pm}$) plane indicates the 95% CL upper limit on the chargino-neutralino production NLO cross section times branching fraction in the flavor-democratic scenario, for the three-lepton search. The contours bound the mass regions excluded at 95% CL for a branching fraction of 50%, as appropriate for the visible decay products in this scenario. The contours based on the observations are shown; in addition, the expected bound is shown.

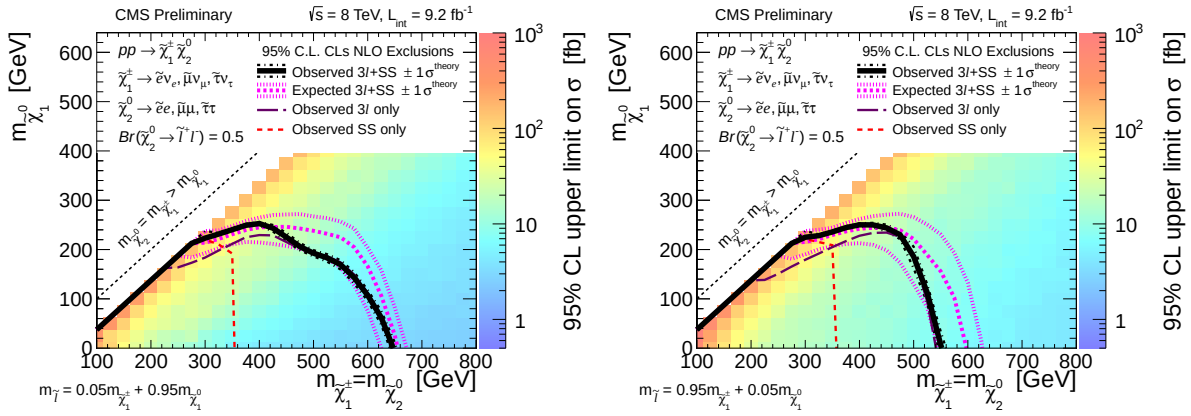

(a) $x_{\tilde{\ell}} = 0.05$ (b) $x_{\tilde{\ell}} = 0.95$

Figure 17: The shading in the $m_{\tilde{\chi}_1^0}$ versus $m_{\tilde{\chi}_2^0}$ ($= m_{\tilde{\chi}_1^\pm}$) plane indicates the 95% CL upper limit on the chargino-neutralino production NLO cross section times branching fraction in the flavor-democratic scenario, for the combined analysis of the three-lepton search and the same-sign dilepton search. The contours bound the mass regions excluded at 95% CL for a branching fraction of 50%, as appropriate for the visible decay products in this scenario. The contours based on the observations are shown for the combination; in addition, the expected combined bound is shown. Other contours show separate mass exclusions for the three-lepton search and the same-sign dilepton search alone.

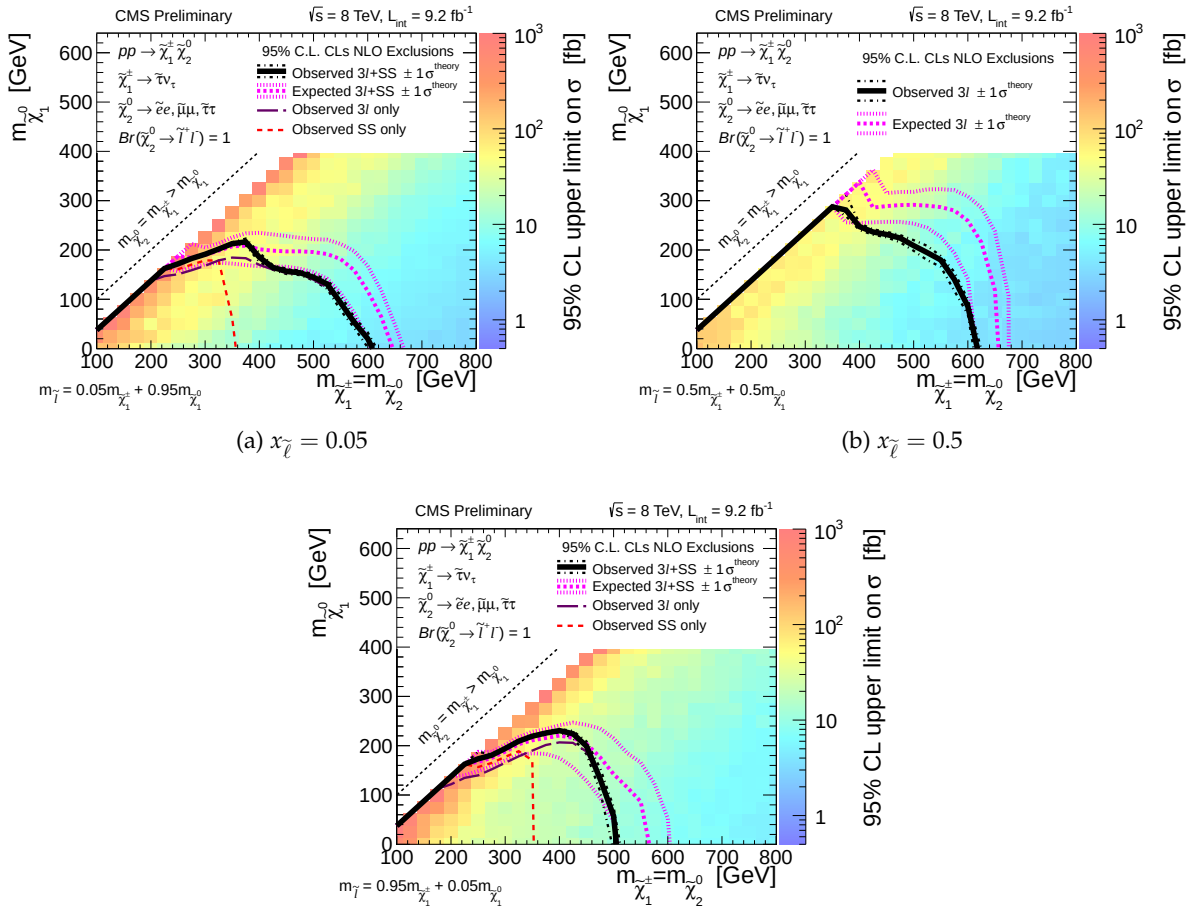

(a) $x_{\tilde{\ell}} = 0.05$

(b) $x_{\tilde{\ell}} = 0.5$

(c) $x_{\tilde{\ell}} = 0.95$

Figure 18: The exclusion contours for the τ-enriched scenario corresponding to the results in Fig. 16, for (a) and (c) the combination of the three-lepton searches with SS dilepton analysis, and (b) the three-lepton searches.

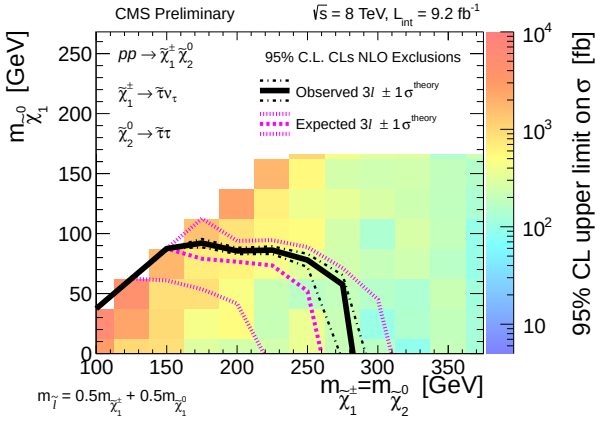

Figure 19: The exclusion contours for τ-dominated scenario corresponding to results in Fig. 16.

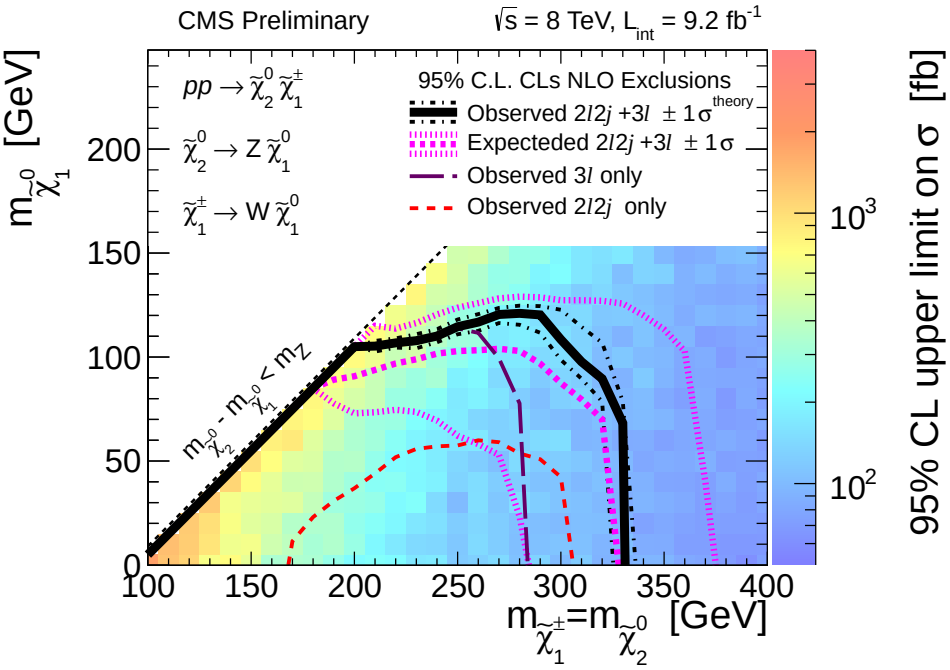

Figure 20: Interpretation of the dilepton WZ + $E_{\mathrm{T}}^{\mathrm{miss}}$ and three-lepton results. The dilepton observed, three-lepton observed, their combination, and combined expected contours are shown.

WZ/ZZ + $E_{\mathrm{T}}^{\mathrm{miss}}$ analysis of Section 6 to restrict the GMSB scenario. The results are displayed in Fig. 21.

8.4 Limits on chargino and slepton pair production

Figure 22 shows limits on the chargino and slepton pair-production cross section times branching ratio for the processes of Fig. 3. The limits for chargino-pair production are set using both the opposite- and same-flavor channels discussed in Section 7, while the limits for slepton pair production are set using only the same-flavor channel.

9 Summary

This note presents searches for supersymmetric charginos, neutralinos, and sleptons. The searches explore final states with three leptons, four leptons, two same-sign leptons, two resonant opposite-sign-same-flavor leptons plus two jets, and two non-resonant opposite-sign leptons. Figure 23 displays four of the results presented above on a single plot. No excesses above the standard model expectations are observed. The results are used to exclude a range of chargino, neutralino, and slepton masses, where we assume these particles have large branching fractions to leptons and vector bosons.

The results improve on the previous CMS search for electroweak supersymmetry [8]. This analysis also presents the first interpretation from CMS of models with slepton and chargino pair production.

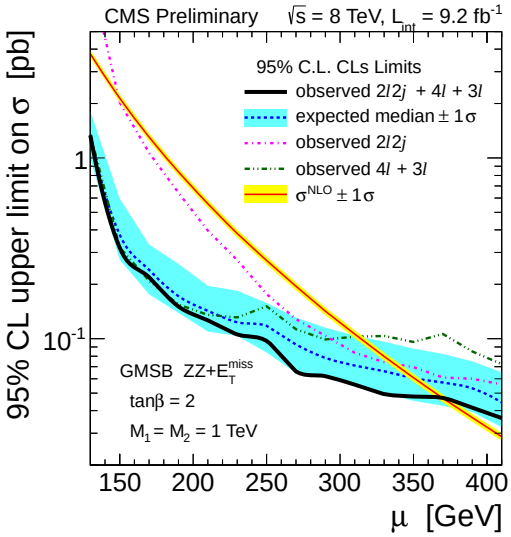

Figure 21: Interpretation of the Z + dijet and four-lepton analyses in the GMSB model discussed in the text. The observed and expected cross section upper limits are indicated as a function of the mass parameter μ, and are compared to the theory cross section. The region $\mu < 370$ GeV is excluded at 95% confidence level.

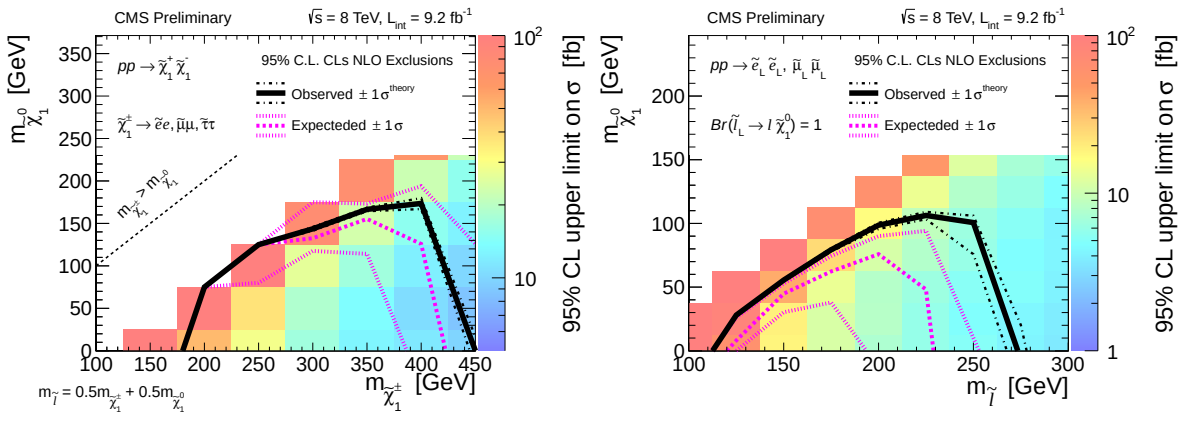

Figure 22: Limits on chargino pair production (left) and slepton pair production (right) cross section times branching ratio for charginos and sleptons decaying as in Fig. 3.

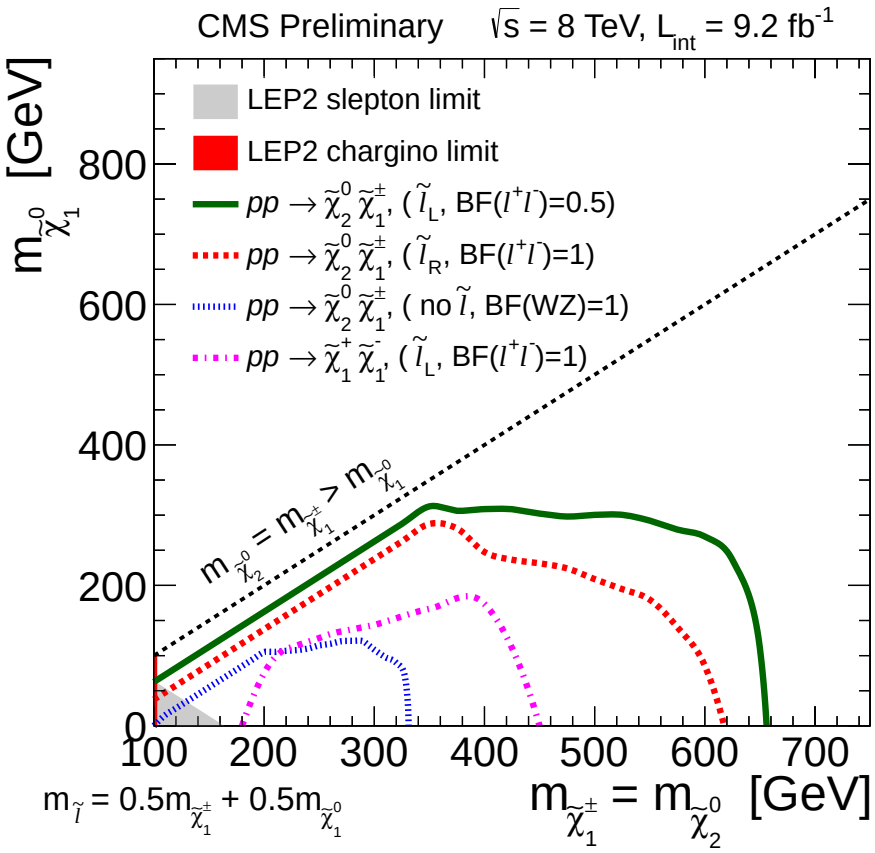

Figure 23: Summary of results for chargino-neutralino production with decays to left-handed sleptons, right-handed sleptons, or direct decays to vector bosons, and chargino-pair production. Where applicable, the $x_{\tilde{\ell}}$ value used to calculate the slepton mass is 0.5.

Acknowledgements

We thank David Shih for useful discussions and help with implementation of the Z-enriched GMSB model of Section 8.3.

References

[1] Y. Golfand and E. Likhtman, "Extension of the algebra of Poincare group generators and violation of p invariance", *JETP Lett.* **13** (1971) 323. Russian version at http://www.jetpletters.ac.ru/ps/717/article_11110.shtml.

[2] P. Ramond, "Dual theory for free fermions", *Phys. Rev. D* **3** (1971) 2415, doi:10.1103/PhysRevD.3.2415.

[3] A. Neveu and J. Schwarz, "Factorizable dual model of pions", *Nucl. Phys. B* **31** (1971) 86, doi:10.1016/0550-3213(71)90448-2.

[4] A. Neveu and J. Schwarz, "Quark model of dual pions", *Phys. Rev. D* **4** (1971) 1109, doi:10.1103/PhysRevD.4.1109.

[5] D. Volkov and V. Akulov, "Is the neutrino a goldstone particle?", *Phys. Lett. B* **46** (1973) 109, doi:10.1016/0370-2693(73)90490-5.

[6] J. Wess and B. Zumino, "A Lagrangian model invariant under supergauge transformations", *Phys. Lett. B* **49** (1974) 52, doi:10.1016/0370-2693(74)90578-4.

[7] J. Wess and B. Zumino, "Supergauge transformations in four-dimensions", *Nucl. Phys. B* **70** (1974) 39, doi:10.1016/0550-3213(74)90355-1.

[8] CMS Collaboration, "Search for electroweak production of charginos and neutralinos using leptonic final states in pp collisions at $\sqrt{s} = 7$ TeV", (2012). arXiv:1209.6620. Accepted by JHEP.

[9] CMS Collaboration, "Search for anomalous production of multilepton events in pp collisions at $\sqrt{s} = 7$ TeV", *JHEP* **06** (2012) 169, doi:10.1007/JHEP06(2012)169.

[10] K. T. Matchev and S. D. Thomas, "Higgs and Z boson signatures of supersymmetry", *Phys. Rev. D* **62** (2000) 077702, doi:10.1103/PhysRevD.62.077702.

[11] P. Meade, M. Reece, and D. Shih, "Prompt decays of general neutralino NLSPs at the Tevatron", *JHEP* **05** (2010) 105, doi:10.1007/JHEP05(2010)105.

[12] J. T. Ruderman and D. Shih, "General neutralino NLSPs at the early LHC", (2011). arXiv:1103.6083.

[13] CMS Collaboration, "The CMS experiment at the CERN LHC", *JINST* **3** (2008) S08004, doi:10.1088/1748-0221/3/08/S08004.

[14] F. Maltoni and T. Stelzer, "MadEvent: automatic event generation with MadGraph", *JHEP* **02** (2003) 027, doi:10.1088/1126-6708/2003/02/027.

[15] J. Alwall et al., "MadGraph 5: going beyond", *JHEP* **06** (2011) 128, doi:10.1007/JHEP06(2011)128.

[16] T. Sjöstrand, S. Mrenna, and P. Skands, "A brief introduction to PYTHIA 8.1", *Comput. Phys. Commun.* **178** (2008) 852, doi:10.1016/j.cpc.2008.01.036.

[17] P. M. Nadolsky et al., "Implications of CTEQ global analysis for collider observables", *Phys. Rev. D* **78** (2008) 013004, doi:10.1103/PhysRevD.78.013004.

[18] J. M. Campbell, R. Ellis, and C. Williams, "Vector boson pair production at the LHC", *JHEP* **07** (2011) 018, doi:10.1007/JHEP07(2011)018.

[19] W. Beenakker et al., "Production of charginos, neutralinos, and sleptons at hadron colliders", *Phys. Rev. Lett.* **83** (1999) 3780, doi:10.1103/PhysRevLett.83.3780.

[20] W. Beenakker et al., "Erratum: production of charginos, neutralinos, and sleptons at hadron colliders", *Phys. Rev. Lett.* **100** (2008) 029901, doi:10.1103/PhysRevLett.100.029901.

[21] M. Krämer et al., "Supersymmetry production cross sections in pp collisions at $\sqrt{s} = 7$ TeV", (2012). arXiv:1206.2892.

[22] P. Z. Skands et al., "SUSY Les Houches accord: interfacing SUSY spectrum calculators, decay packages, and event generators", *JHEP* **07** (2004) 036, doi:10.1088/1126-6708/2004/07/036.

[23] H. Baer et al., "Simulating supersymmetry with ISAJET 7.0 / ISASUSY 1.0", (1993). arXiv:hep-ph/9305342.

[24] W. Beenakker, R. Hoepker, and M. Spira, "PROSPINO: a program for the production of supersymmetric particles in next-to-leading order QCD", (1996). arXiv:hep-ph/9611232.

[25] S. Agostinelli et al., "GEANT4 – a simulation toolkit", *Nucl. Instr. Meth. A* **506** (2003) 250, doi:10.1016/S0168-9002(03)01368-8.

[26] CMS Collaboration, "The fast simulation of the CMS Detector at the LHC", in *International Conference on Computing in High Energy and Nuclear Physics (CHEP 2010). J. Phys.: Conference Series* 331 (2011) 032049. doi:10.1088/1742-6596/331/3/032049.

[27] CMS Collaboration, "Study of tau reconstruction algorithms using pp collisions data collected at $\sqrt{s} = 7$ TeV", CMS Physics Analysis Summary CMS-PAS-PFT-10-004, (2010).

[28] CMS Collaboration, "CMS strategies for tau reconstruction and identification using particle-flow techniques", CMS Physics Analysis Summary CMS-PAS-PFT-08-001, (2009).

[29] CMS Collaboration, "Electron reconstruction and identification at $\sqrt{s} = 7$ TeV", CMS Physics Analysis Summary CMS-PAS-EGM-10-004, (2010).

[30] CMS Collaboration, "Performance of CMS muon reconstruction in pp collision events at $\sqrt{s} = 7$ TeV", (2012). arXiv:1206.4071. Submitted to *JINST*.

[31] M. Cacciari, G. P. Salam, and G. Soyez, "The anti-k_t jet clustering algorithm", *JHEP* **04** (2008) 063, doi:10.1088/1126-6708/2008/04/063.

[32] M. Cacciari and G. P. Salam, "Pileup subtraction using jet areas", *Phys. Lett. B* **659** (2008) 119, doi:10.1016/j.physletb.2007.09.077.

[33] CMS Collaboration, "Performance of the b-jet identification in CMS", CMS Physics Analysis Summary CMS-PAS-BTV-11-001, (2011).

[34] CMS Collaboration, "Search for new physics with same-sign isolated dilepton events with jets and missing transverse energy", (2012). arXiv:1205.6615. Submitted to *Phys. Rev. Lett.*

[35] CMS Collaboration, "Performance of τ lepton reconstruction and identification in CMS", *JINST* **7** (2012) P01001, doi:10.1088/1748-0221/7/01/P01001.

[36] CMS Collaboration, "Measurement of the inclusive W and Z production cross sections in pp collisions at $\sqrt{s} = 7$ TeV with the CMS experiment", *JHEP* **10** (2011) 132, doi:10.1007/JHEP10(2011)132.

[37] CMS Collaboration Collaboration, "Search for physics beyond the standard model in events with a Z boson, jets, and missing transverse energy in pp collisions at $\sqrt{s} = 7$ TeV", *Phys. Lett.* **B716** (2012) 260–284, doi:10.1016/j.physletb.2012.08.026, arXiv:1204.3774.

[38] K. T. Matchev and M. Park, "A General method for determining the masses of semi-invisibly decaying particles at hadron colliders", *Phys. Rev. Lett.* **107** (2011) 061801, doi:10.1103/PhysRevLett.107.061801, arXiv:0910.1584.

[39] D. R. Tovey, "On measuring the masses of pair-produced semi-invisibly decaying particles at hadron colliders", *JHEP* **0804** (2008) 034, doi:10.1088/1126-6708/2008/04/034, arXiv:0802.2879.

[40] T. Junk, "Confidence level computation for combining searches with small statistics", *Nucl. Instrum. Meth. A* **434** (1999) 435, doi:10.1016/S0168-9002(99)00498-2.

[41] A. L. Read, "Presentation of search results: The CL_s technique", *J. Phys. G* **28** (2002) 2693, doi:10.1088/0954-3899/28/10/313.

[42] ATLAS and CMS Collaborations, "Procedure for the LHC Higgs boson search combination in summer 2011", Technical Report ATL-PHYS-PUB-2011-11, CMS-NOTE-2011-005, Geneva, (2011).